Journal of Energy Storage 119 (2025) 116238

Contents lists available at ScienceDirect

Journal of Energy Storage

journal homepage: www.elsevier.com/locate/est

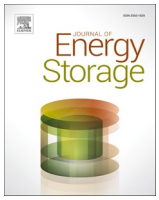

Research Papers

# Impact of humidity on moisture resorption and resulting electrochemical performance of Gr/NMC622-based Li-ion batteries

Hans Fenske [a,b,*], Thilo Heckmann [c], Peter Michalowski [a,b], Philip Scharfer [c], Wilhelm Schabel [c], Arno Kwade [a,b]

[a] Institute for Particle Technology, Technische Universität Braunschweig, Volkmaroder Straße 5, 38104 Braunschweig, Germany
[b] Battery LabFactory Braunschweig, Technische Universität Braunschweig, Langer Kamp 19, 38106 Braunschweig, Germany
[c] Karlsruhe Institute of Technology, Thin Film Technology, Straße am Forum 7, 76131 Karlsruhe, Germany

ARTICLE INFO

*Keywords:*
Lithium-ion batteries
Battery production
Moisture management
Residual moisture analysis
Cell performance

ABSTRACT

Moisture management is an integral part of modern battery production. However, there is only little information available about the level of humidity in the production environment after which detrimental effects on cell performance set in. In this study, we investigate the impact of industry relevant levels of humidity on moisture resorption and electrochemical performance of Gr/NMC622-based Li-ion batteries utilizing two types of separator (one polyolefin and one with ceramic coating). The moisture resorption behaviour of all cell components was analysed in detail using Karl Fischer titration (KFT) and a magnetic suspension balance. The electrochemical performance was evaluated using PAT-cells that were assembled under identical humidity conditions and in parallel with the KFT sample preparation. We found a stable electrochemical performance for low dew points and an increase in irreversible capacity and internal resistance once a critical dew point was exceeded. By correlating residual moisture data and electrochemical performance, a common critical residual moisture content could be identified. The presented method allows, for the first time, to quantify the impact of residual cell moisture on electrochemical performance with high precision.

## 1. Introduction

It is widely recognized that water can have a detrimental effect on the performance and safety of lithium-ion batteries (LIBs). Consequently, effective moisture management is a crucial aspect of modern battery production [1–3]. Some LIB cell components display a high degree of reactivity towards water, resulting in significant material degradation if they are exposed to humidity during the storage or processing of the materials [4–17]. However, water from ambient humidity can be absorbed by all cell components, increasing their moisture content and thereby subsequently introducing water into the battery cell [18–27]. Once inside the battery cell, the water may induce unwanted side reactions during battery operation.

The cell components that are most susceptible to direct reaction with water are the electrolyte and the cathode active material (CAM). The commonly used Li-salt $LiPF_6$ can react with water, resulting in the formation of hydrofluoric acid (HF) [4–7]. This reaction takes place rapidly even at ambient temperature, resulting in a transformation of $H_2O$ into HF at a ratio of 1:2 [5,7]. While HF itself is a dangerous side-product, it can also have a detrimental impact on battery performance by facilitating further reactions with the solid electrolyte interphase (SEI) or the cathode electrolyte interphase (CEI) and the CAM once introduced into the battery cell [28–30]. Furthermore, CAMs that are based on Ni-rich transition metal oxides like $LiNi_xMn_yCo_zO_2$ (NMC) and $LiNi_xCo_yAl_zO_2$ (NCA) are known to degrade when exposed to ambient air. Due to their high specific capacity, there is an ongoing market transition towards Ni-rich CAM [31,32], which results in a continuous research interest regarding their atmospheric stability. Decreasing electrochemical performance after prolonged exposure to humid air has been shown for NMC523 [8], NMC622 [9,10], NMC811 [11,12], NMC851005 [13] and NCA [14,15]. It has been shown that the degradation of nickel rich CAM requires the presence of $H_2O$ as well as $CO_2$ [33,34] and the observed performance decrease is often attributed to the formation of reaction layers consisting of LiOH and $Li_2CO_3$. Lou et al. visualized the formation of a passivating LiOH-layer on top of NMC811 after exposure to water vapour by cross-sectional high-resolution environmental transmission

* Corresponding author at: Institute for Particle Technology, Technische Universität Braunschweig, Volkmaroder Straße 5, 38104 Braunschweig, Germany
*E-mail address:* hans.fenske@tu-braunschweig.de (H. Fenske).

https://doi.org/10.1016/j.est.2025.116238
Received 21 October 2024; Received in revised form 11 March 2025; Accepted 12 March 2025
Available online 26 March 2025

electron microscopy [16]. This passivating LiOH layer further reacted to $Li_2CO_3$ in the presence of $CO_2$, which may explain the continuous degradation observed by other studies. Indeed, the majority of studies investigating CAM degradation have been conducted under ambient conditions or in even more extreme conditions to accelerate the ageing process. In a recent study, Lechner et al. tested the critical moisture exposure duration of very high nickel NMC (91 mol% nickel) under industry-relevant dry room conditions for the first time [17]. Interestingly, they found no significant impact on electrochemical performance after a multiday storage at a dew point of around −25 °C. This finding highlights that the degradation of CAMs occurs over significantly longer time periods than the adsorption of residual water.

In the production of batteries, the process of post-drying, also known as final drying or electrode/stack baking, is commonly employed to reduce the residual moisture content of cell components [1,20,21]. It is essential that all subsequent process steps occur within a dry room environment to prevent remoistening and ensure that the post-dried components retain a sufficiently low residual moisture content. Kosfeld et al. presented a comprehensive overview of various post-drying techniques and moisture management strategies employed throughout the production process [20]. The moisture adsorption potential of each cell component is mainly determined by the adsorption behaviour of the individual materials within the component. A mixture of carboxymethyl cellulose (CMC) and styrene-butadiene rubber (SBR) is typically utilized as binder material in state-of-the-art aqueous processed graphite (Gr) anodes [31]. However, CMC is the component that absorbs the highest amount of moisture among all battery materials [20]. For this reason, the water uptake behaviour of CMC-containing Gr anodes was extensively studied in the past [18,19,35]. NMC-based cathodes generally exhibit a lower moisture content than CMC-containing Gr anodes and their moisture content is mainly determined by the water adsorption of the CAM itself rather than by the water uptake of the commonly used binder PVDF [20,35]. The formation of hydrates in LiOH has been proposed as a possible sorption mechanism in NMC, which results in a significant increase in water uptake compared to the water uptake solely caused by physically adsorbed water at the surface of the CAM [36]. The water adsorption of separators can either be very low compared to other cell components, in the case of polyolefin separators, or in the same range as CMC-containing Gr anodes, in the case of separators containing ceramic particles [20,37]. For all cell components a hysteresis behaviour after post-drying was shown, leading to lower moisture contents during moisture resorption compared to moisture desorption [18,21]. An efficient design of post-drying procedures therefore requires know-how of the individual equilibrium conditions as well as the sorption kinetics of each cell component [21,35].

Once assembled into a battery cell, all cell components are connected by the electrolyte, which allows for the transfer of water from each cell component into the electrolyte. This may cause unwanted side reactions like HF formation [4,5], decomposition of water at the electrodes under battery operation conditions [38], and hydrolysis of electrolyte solvents, such as ethylene carbonate [39], resulting in changes to the SEI and CEI formation as well as the generation of excessive gassing. While it is widely accepted that an excessive water content is detrimental to battery safety and performance, there is a lack of information regarding the threshold at which detrimental effects set in. Burns et al. even found positive effects on the electrochemical performance of prismatic Gr/$LiCoO_2$, Gr/NMC and $LiCoO_2$/$Li_4Ti_5O_{12}$ cells upon the addition of up to 1000 ppm water as electrolyte additive [40,41]. In a similar study Xiong et al. found no detrimental effects on the electrochemical performance of Gr/$LiCoO_2$ pouch cells for up to 2000 ppm water [42]. In contrast, Zheng et al. reported a range of detrimental effects on the performance of 18650-type Gr/NMC cylindrical cells after intentionally injecting deionized water into the cell [43]. They reported an immediate reduction in initial charge voltage, initial capacity, capacity retention and an increase in internal resistance following the addition of two or more milligrams of water. Although it is common to investigate the effect of water by adding water directly into the electrolyte/cell [29,30,38–40,42,43], this does not accurately reflect the real-world scenario, where water levels in the electrolyte are typically strictly controlled [4] and water is introduced primarily through residual moisture in cell components [20]. The advantage of adding water via the electrolyte is that it allows for precise control of the water content. In contrast, controlling and measuring the water content in cell components is much more challenging due to fast ad- and desorption kinetics. While previous studies, which have investigated the effect of residual moisture on cell performance by variations in post-drying conditions, have yielded valuable general insights, they often did not account for water adsorption and desorption during cell assembly and have not reported the moisture contents of all major cell components [23–26].

Reliable methods for water content determination are essential for the analysis and optimisation of moisture management strategies. Coulometric Karl Fischer titration (KFT) is a technique commonly employed to determine the water content of battery materials [4,20,23,27,30,37,38,44–47]. For solid materials, such as electrodes and separators, the indirect KFT method is employed. A detailed discussion of various test procedures for indirect KFT was given by Kosfeld et al. [27] and Stich et al. [37]. In essence, the method detects the amount of water that is evaporated from a sample at a given oven temperature. The magnetic suspension balance (MSB) is an instrument used to study sorption phenomena in various fields of research [48–51]. The uptake of moisture in battery materials can also be measured using an MSB [18–20,35,36]. Test samples are conditioned and measured in a sealed, humidity- and temperature-controlled cell and the mass change of the sample is detected gravimetrically in real time. This direct detection of water uptake also allows the investigation of kinetic effects.

This study examines the moisture resorption behaviour of CMC-containing Gr anodes, NMC622 cathodes and two different types of separator (polyolefin and ceramic particle containing) under industrially relevant levels of humidity. NMC622 was chosen as CAM for this study because NMCs are currently the most widely utilized CAM in electric vehicles [32,52]. According to the International Energy Agency, NMCs with medium Ni content, such as NMC622 and NMC532, collectively accounted for more than one third of the total market share in 2022 [52]. The water uptake and residual moisture of all materials are quantified using a magnetic suspension balance (MSB) and Karl Fischer titration (KFT). Laboratory-scale, three-electrode test cells were assembled using the intentionally moisturised cell components and were analysed for their formation behaviour, C-rate capability, internal resistance and cycling stability.

## 2. Materials and methods

### 2.1. Materials and electrode manufacturing

Table 1 provides an overview of all the materials used in this work, including the electrode recipe. The cathode slurry preparation was conducted using a planetary mixer (PMH 10, NETZSCH Feinmahltechnik GmbH) with a batch size of 3.5 l. The mixer was equipped with a highspeed stirrer (hss) with double butterfly setup, a cross-beam low-speed stirrer (lss) and a rotating baffle as wall scraper. Dispersing was carried out in a five-step process: 1) mixing of all dry components (NMC622, PVDF, C65, SFG6L); 2) addition of N-Methyl-2-pyrrolidone (NMP) (BASF) up to a solids content of 83 %; 3) mixing at 600 rpm (hss) and 100 rpm (lss) for 30 min; 4) addition of NMP up to a solids content of 75 %; 5) mixing for an additional 30 min. The anode slurry was prepared using a dissolver (Dispermat CA60, VMA-Getzmann GmbH) with a batch size of 600 ml and a final solids content of 50 wt.%. Dispersing was carried out in a two-step process using a 50 mm tooth disk: 1) dispersion of the powder mixture (graphite, carbon black, CMC) at a tip speed of 9 m $s^{-1}$ for 45 min; and 2) addition of SBR-solution and degassing at 3 m $s^{-1}$ for 15 min. A continuous lab coater (LabCo, Kroenert GmbH & Co. KG) was used for coating and drying of all electrodes. A 20 μm thick

**Table 1**
Overview of cell components and electrode recipe used in this work.

| Material | Function | Type & supplier | Mass fraction [%] |
|---|---|---|---|
| **Cathode** | | | |
| NMC | Active material | NMC622, BASF SE | 95.50 |
| Polyvinylidene fluoride | Binder | Solef 5130, Solvay | 2.25 |
| Carbon black | Conductive additive | C-Nergy C65, Imerys Graphite & Carbon | 1.50 |
| Graphite | Conductive additive | TIMREX SFG6L, Imerys Graphite & Carbon | 0.75 |
| **Anode** | | | |
| Graphite | Active material | Artificial graphite | 94.00 |
| Carboxymethyl cellulose | Binder | 2000PA, DOW Chemical | 2.00 |
| Styrene-butadiene rubber | Binder | BM-451B, Zeon Europe | 3.00 |
| Carbon black | Conductive additive | C-Nergy C65, Imerys Graphite & Carbon | 1.00 |
| **Separator** | | | Thickness: |
| PP fiber/PE membrane | Polyolefin separator | FS-5P, EL-Cell | 220 µm |
| Polyester non-woven with ceramic coating | Ceramic separator | OZ-S30, Mitsubishi Paper Mills | 30 µm |

aluminium foil (Hydro Aluminium GmbH) and a 10 µm thick copper foil (Sumitomo Electric Hartmetall GmbH) were used as substrates for the cathode and anode, respectively. The coating speed and drying temperature were set at 2 m $min^{-1}$ and 80/100/120 °C for the cathode and 1.5 m $min^{-1}$ and 60/60/60 °C for the anode. A two-roll compactor (GKL400, Saueressig GmbH und Co. KG) was used to adjust the final density of the electrodes.

The final mass loading and density of the electrodes were 16 mg $cm^{-2}$ and 3.0 g $cm^{-3}$ for the cathode and 9 mg $cm^{-2}$ and 1.3 g $cm^{-3}$ for the anode. Following the recommendations by Kasnatscheew et al. [53], the electrode capacity balancing (a/c ratio) was calculated based on the initial charge capacities of each electrode. Assuming an initial charge capacity of 190 mAh $g^{-1}$ for the cathode and 385 mAh $g^{-1}$ for the anode, this yields an a/c ratio of approximately 1.1 for all cells used in this work.

### 2.2. Post-drying and controlled moisture exposure

For controlled moisture exposure, an argon-filled glovebox system from GS Glovebox Systemtechnik GmbH was used. Prior to moisture exposure, all electrodes and separators were post-dried inside the antechamber of the glovebox. The post-drying procedure was based on the work of Huttner et al. [21]. For the present study, no preheating phase was used as only sheet material was processed. During the 6-h vacuum-drying, the pressure was maintained below 25 mbar, with argon purging cycles every 15 min. The process was conducted at 80 °C for electrodes and 50 °C for separators. After transfer into the glovebox, all materials were sealed in pouch bags under dry conditions. In the context of this study, the term “dry conditions” refers to the standard operation mode of the glovebox, in which water and oxygen filters are activated. Prior to controlled moisture injection, the water filters are deactivated, while the oxygen filters remained operational. Consequently, the oxygen levels inside the glovebox were below 1 ppm at all times. The dew point inside the glovebox was measured utilizing a Vaisala DRYCAP 180 M Dew point Transmitter with a measurement range of −60 °C to +60 °C dew point temperature and an accuracy of ±2 °C. At dry conditions, the dew point was below the measurement range, which is why results gathered under dry conditions are arbitrarily displayed in place of a dew point of −70 °C.

The moisture content inside the glovebox was adjusted by injecting moisture-saturated Argon into the glovebox atmosphere. A fan-coupled heat exchanger located at the ceiling of the box ensured a uniform temperature and moisture distribution. During exposure, the dew point was regulated to always be within ±1 °C of the target value. The temperature within the glovebox was maintained at 25 °C ± 0.5 °C throughout this study. To ensure sufficient time for each material to reach equilibrium conditions, an exposure duration of minimum 12 h was selected. All materials used for the KFT measurements and cell assembly, including the insulation sleeves with built-in separators and the cell casings, were exposed in parallel. The electrolyte was not intentionally exposed to moisture (see Section 2.4).

### 2.3. Determination of water content

The water content of anode, cathode and separators was determined using KFT and a MSB. The experimental set-up for both measurement techniques is presented in Fig. 1. The sample preparation was conducted under ambient atmosphere for both methods. The KFT measurements were conducted in the Battery LabFactory Braunschweig (Technical University of Braunschweig), while the MSB measurements were carried out at the Institute for Thin Film Technology (Karlsruhe Institute of Technology). For storage and shipping, the sample materials were sealed in pouch bags under argon atmosphere.

#### 2.3.1. Measurement of water content using KFT

For KFT an AQUA 40.00 from ECH Elektrochemie Halle GmbH equipped with a headspace oven module was employed. During a measurement, the headspace vial containing the sample material is placed inside the oven module. The septum of the vial is punctured with a twin-hole needle and the sample material is flushed with a carrier gas. The carrier gas is circulated in a closed circuit between the measuring cell and the needle head in the headspace vial. In this study, the oven temperature was set to 120 °C and the measurement time was set to 20 min for all materials. For each measurement point and material, three samples were analysed. Blank values were taken with the same measurement routine before and after each set of three samples. The KFT device is situated within a dry room with a dew point temperature of −20 °C.

#### 2.3.2. Measurement of water content using a MSB

The MSB measures sorption equilibria gravimetrically with a resolution of up to 10 µg [18,19]. The sample is confined in a conditioned measurement cell that is sealed towards the environment [54]. All samples were pre-treated with the same temperature profile used for the post-drying before KFT sampling. A gas mixture facilitates the conditioning of the measurement cell via combining a saturated with an unsaturated, dry (dew point around −65 °C) nitrogen stream at various ratios [55]. Depending on this ratio, the relative humidity adjusts in the measurement cell, which is monitored by a chilled-mirror dew-point indicator. The temperature inside the measurement cell was kept at 25 °C ± 0.1 °C during the experiments. The weight of the sample as a function of the relative humidity is determined until the weight is constant over time (weight change $<2 \times 10^{-5}$ g $h^{-1}$ over a period of 6 h). The dry mass for each sample is defined as the mass that is measured at a dew point of −65 °C sample temperature.

### 2.4. Cell assembly and electrochemical characterization

Cell testing was conducted using PAT-Cells from EL-Cell GmbH in two- and three-electrode configuration. Circular stamps with a diameter of 18 mm were used for anode and cathode (no anode overhang). Cell assembly was conducted within the humidity-controlled glovebox system. For cells with the ceramic separator the insulation sleeve was assembled by hand, for cells with the polyolefin separator the insulation sleeve (including a Li-ring reference) was taken from EL-Cell GmbH. For

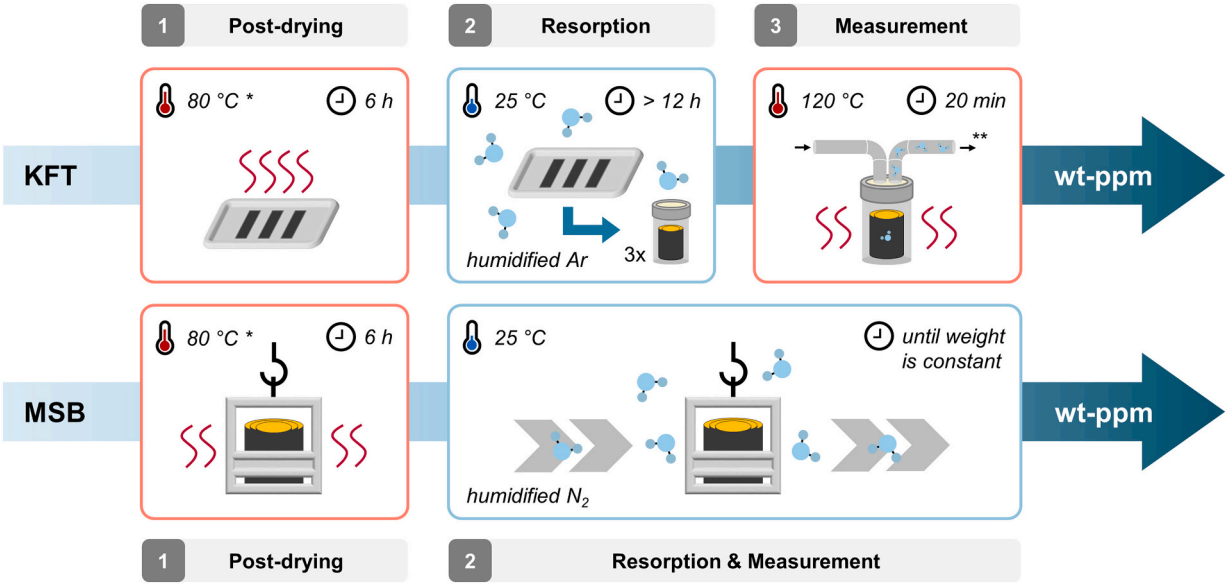


**Fig. 1.** Experimental set-up used for the water content determination with Karl Fischer titration (KFT) and magnetic suspension balance (MSB). The two methods differ in their testing procedure, but both can be subdivided into three parts: post-drying, moisture resorption and moisture measurement. For the KFT, the sample material is transferred between different locations during the testing procedure, while for the MSB, it remains inside the same measurement cell. Post-drying temperatures are identical for both methods with 80 °C for anode/cathode and (*) 50 °C for both separator types. During the KFT measurement, (**) the carrier gas is circulated in a closed circuit.

every dew point and separator combination, four test cells were constructed. To minimize the effects of potential moisture contamination of the electrolyte, the electrolyte was stored in a separate glovebox ($H_2O$ and $O_2$ levels <1 ppm). The electrolyte was distributed into small aluminium bottles and transferred into the humidity-controlled glovebox only prior to cell assembly. For every set of four test cells, a new bottle was opened, and the time between the opening of the bottle and the closure of all cells was less than 5 min. Cells with polyolefin separator were filled with 100 µl of electrolyte and cells with ceramic separator were filled with 80 µl of electrolyte. The electrolyte composition was identical for all cells (1 M $LiPF_6$ in EC:EMC (3:7 by wt%) + 2 wt% vinylene carbonate (VC), E-Lyte Innovations GmbH). All cells were tested utilizing a CTS LAB battery test system from BaSyTec GmbH. Two different cycling procedures were employed for the dew point screening and cycle life investigation. The initial three cycles were identical for both test procedures and included a direct current internal resistance (DCIR) test subsequent to the third cycle. For the dew point screening, the DCIR test was followed by a charge rate test, while for the cycle life investigation, a long-term cycling under 1 C/1 C was applied. A charge rate test allows to determine the charging performance of a test cell without interference from the discharge step. The charging performance is considered to be crucial for many mobility applications like electric vehicles [56,57]. The exact test procedures are outlined in Table 2. Due to the inherent challenges with building laboratory scale test cells with thin separators, the failure rate of the test cells with the ceramic separator (thickness: 30 µm) was higher than the failure rate of the cells with the polyolefin separator (thickness: 220 µm). Consequently, only three cells with ceramic separator could be evaluated for most tests (only one cell in case of DCIR and charge rate test at −60 °C dew point).

**Table 2**
Overview of cycling procedures (cut-off voltages: 2.9 V to 4.2 V).

| Dew point screening | Cycle life investigation |
|---|---|
| **Formation:** | |
| 1 × 0.1 C/0.1 C (CCCV till 0.05 C) | |
| **Check-up:** | |
| 2 × 0.2 C/0.2 C (CCCV till 0.05 C) | |
| **Direct current internal resistance test (DCIR):** | |
| charge to 50 % SOC; 1 h rest; 10 s pulse at 1 C in charge direction | |
| **Charge rate test:** | **Cycling:** |
| Charge: 3 × 0.5 C/1 C/2 C/3 C (CC) | 100× 1 C/1 C (CC) |
| Discharge: 0.2 C with CCCV till 0.05 C | **Check-up + DCIR** |
| | (Looped 5× with cycling step) |

## 3. Results and discussion

### 3.1. Moisture resorption of cell components under controlled humidity

Determining the moisture content of cell components is crucial to analyse the effect of the humidity in the production atmosphere on the cell performance. The moisture content helps to identify critical cell components that either carry large amounts of water into the cell or deteriorate due to exposure to humidity. In this study, two methods for determining moisture content are employed and subsequently compared to one another: indirect coulometric Karl Fischer titration and magnetic suspension balance. Prior work by Kosfeld et al. also employed both methods, but no comprehensive comparison was attempted due to discrepancies in the sample handling prior to the respective measurements [20]. To ensure a valid comparison in this study, the post-drying and moisture resorption were conducted under comparable conditions for both methods (see Fig. 1).

A meaningful comparison of the two methods requires a precise consideration of the respective measuring principles. In case of the MSB, moisture resorption and measurement take place simultaneously. The water content is determined directly from the difference between the mass of the sample at each dew points and a dry reference mass. Each dew point is held constant until equilibrium is reached, resulting in a sorption isotherm. In case of the KFT, moisture resorption and measurement take place successively. Following moisture resorption, the water content is detected indirectly by measuring the amount of water

that is released from the sample while it is heated inside the oven module of the KFT. The measurement conditions of each method are a direct consequence of their measurement principle and need to be taken into account when comparing both methods.

Neither method provides an absolute water content of the analysed sample. Instead, both methods quantify the amount of water above their respective reference condition. For MSB, the reference condition equals the dry mass of the sample. For KFT, the reference condition equals the equilibrium between the humidity in the measurement atmosphere and the sample at the given KFT oven temperature. In the context of purely physical sorption processes, the difference in measured water content should be primarily influenced by the variation in relative humidity between these reference conditions. For more strongly bound water, such as hydrates or chemisorbed water, the variation in measurement temperature can lead to a significantly more pronounced effect on the measurement outcome.

Fig. 2 shows the water content and mass uptake of the graphite anodes, NMC cathodes, and two kinds of separator as a function of humidity in form of the dew point temperature. As expected, the water content rises with increasing dew point. The results for both measurement techniques indicate similar trends, however, the results from the KFT measurement show consistently higher absolute values compared to the MSB measurements. As anticipated, the anode exhibits the greatest water uptake, followed in descending order by the ceramic separator, the cathode, and the polyolefin separator. The relative offset between the methods is smallest for the anode and considerably higher for the ceramic separator (absolute offset at −40 °C dew point: 385 ppm) and the cathode. The KFT-results from the cathode also suggest a linear dependency with the dew point, while the MSB-results show an exponential one. In the case of the polyolefin separator, only a minimal water uptake was observed. In this range, both measurement methods operate in close proximity to their respective sensitivity limits, resulting in a considerable degree of scatter in the results for low dew points up to −20 °C.

Given that the humidity-exposure history of the materials is similar for KFT and MSB measurements, the offset between both methods must be attributed to the different measurement conditions. These are: (i) a different relative humidity in the measurement atmosphere, (ii) a different measurement temperature, and (iii) adsorption versus desorption of water. The observed offset is approximately one order of magnitude higher than any offset that could be attributed solely to differences in relative humidity. Therefore, other effects must evoke the difference in measurements. The distinction between adsorption and desorption of water could potentially influence the measurement results. However, this would result in lower values for the KFT compared to the MSB, which is in stark contrast to the observed measurement results. Therefore, it can be assumed that the offset between KFT and MSB is predominantly a function of the different measurement temperatures.

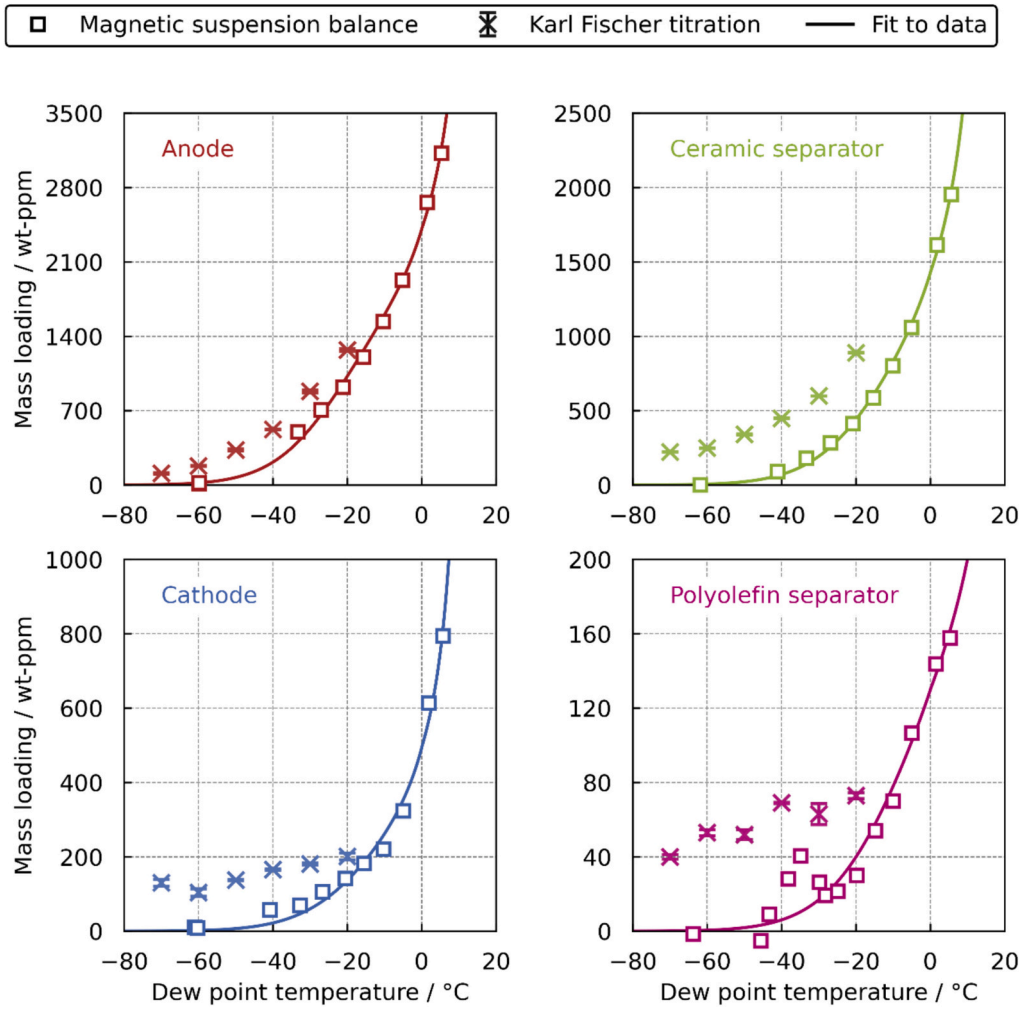


**Fig. 2.** Water uptake of cell components as a function of the dew point, measured by Karl Fischer titration (KFT) and magnetic suspension balance (MSB). The trends of both methods are similar. However, the absolute values differ. The KFT results represent the average and standard deviation of three measurements, while the MSB results are gathered on the same sample that was held at each dew point until a constant weight was achieved. The KFT dry reference (no deliberate remoistening after post-drying) was arbitrarily displayed at −70 °C dew point (dew point sensor out of measurement range).

The small yet consistent offset observed for the anode may be attributable to the temperature-dependent sorption equilibrium of water in CMC [18]. The significant offset detected for the ceramic separator could indicate that additional mechanisms beyond physical sorption contribute to the water uptake. If we assume the formation of species with more strongly bound water, such as hydrates, in the ceramic particles, this sorption may not be fully reversed by the post-drying at 80 °C and therefore be visible in the KFT and not the MSB. The water sorption in NMC is also complex, with a continuous temperature-dependent desorption of water for temperatures up to above 1000 °C [11]. Hydrate formation in LiOH-containing degradation layers on the surface of NMC particles has been proposed as explanation for increased water uptake of NMC in otherwise inert atmosphere [36]. Accordingly, one explanation for the offset between the results of KFT and MSB may be the same as for the ceramic separator. Furthermore, it is possible that the cathode samples do not reach an equilibrium in the KFT measurement (measurement time 20 min). However, the observation of a linear trend in the KFT in comparison to an exponential trend in the MSB is still unexplained and requires further investigation.

Despite the inherent difficulties in comparing residual moisture data from different studies due to variations in sample handling, measurement parameters and material composition, it is reasonable to expect similar results for samples with similar humidity-exposure history and composition. For the purpose of comparison, data from Huttner et al., Eser et al., and Kosfeld et al. were used as a reference [19, 20, 22]. The results of the graphite anode with a CMC/SBR binder system are comparable across all studies, if the CMC-content is considered adequately. Eser et al. found that the anode water uptake scales with the CMC-content. The data for the ceramic separator are strikingly similar to those presented by Kosfeld et al. However, there is no information regarding the type of the ceramic separator used in their study, and therefore this result could be coincidental. The cathode's water uptake presented by Kosfeld et al. and Huttner et al. is lower compared to the water uptake observed in this work [20,22]. It appears that the increased water uptake of NMC622 observed in a previous study for a relative humidity above 30 % occurs at a much lower dew point for the material used in this study [36]. At this point, we do not have a satisfying explanation for the observed large variations in water uptake behaviour for NMC622 cathodes. Exact values are listed in Table S1 in the supplementary material.

In summary, the offset between KFT and MSB was detected for samples even with a comparable humidity-exposure history. This offset

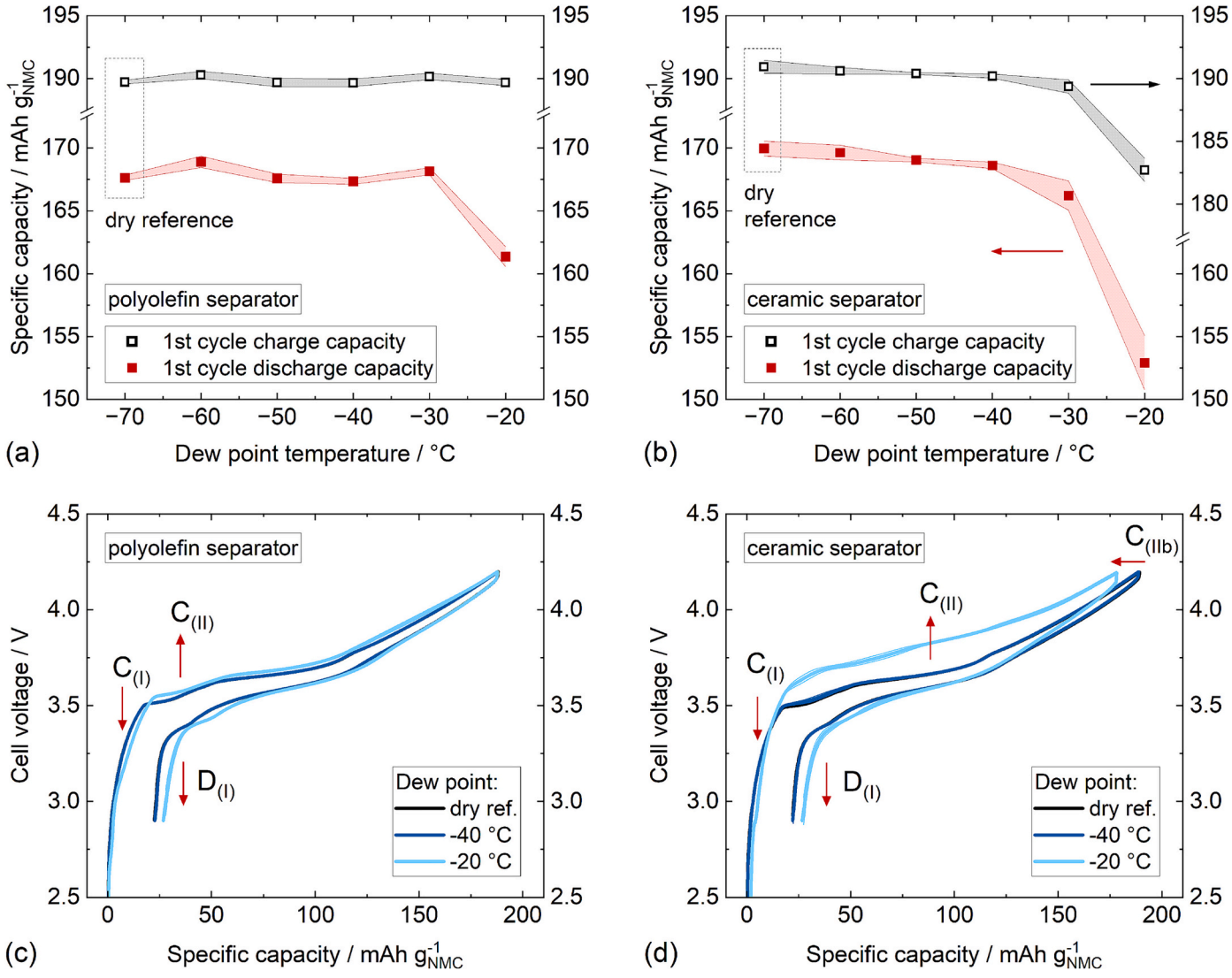


**Fig. 3.** First cycle performance of PAT-cells assembled at varying dew points under humidified argon. The specific charge and discharge capacity of the first cycle, as well as the respective cell voltage curves, are displayed for cells assembled with polyolefin separator (a, c) and ceramic separator (b, d). Each data point and cell voltage curve represents the average and standard deviation from at least three cells.

was smallest for the anode, where physical sorption mechanisms occur. Larger offsets occurred in cathodes and ceramic separator, where hydrate formation and chemical sorption is possible. The comparison to literature data showed consistency, except for the cathode. The results show that measuring an exact moisture content of a cell component is challenging and depends on measurement parameters and technique. For practical application in moisture management, it is important to quantify the impact of the resorbed moisture on the performance of LIB, which will be assessed in the following.

### 3.2. Electrochemical performance after cell assembly under controlled humidity

In order to gain insight into the consequences of varying levels of residual moisture on electrochemical performance, test cells were assembled in parallel with the KFT sample preparation at each investigated dew point. Cells assembled under dry conditions, without any deliberate remoistening, are referred to as "dry reference". The results for the dry reference are arbitrarily displayed in place of −70 °C dew point, because the dew point sensor used within the glovebox for controlled moisture exposure does not deliver reliable data for dry conditions. The results of the first charge/discharge cycle are presented in Fig. 3. The development of the specific charge/discharge capacity demonstrates that an increase in dew point does not result in an immediate reduction in cell performance. Instead, the data indicates a plateau-like behaviour for low dew points in which the dew point has only minimal effect. Interestingly, cells with ceramic separator show a small yet steady decrease of capacity, while cells with polyolefin separator show no clear trend. However, above a dew point of −30 °C for cells with polyolefin separator and − 40 °C for cells with ceramic separator, the discharge capacity decreases significantly for both separator types. Notably, cells assembled with ceramic separator exhibit a simultaneous decrease in both charge and discharge capacity. In contrast, cells assembled with polyolefin separator display a stable charge capacity for all investigated dew point temperatures.

The cell voltage curves of the initial charge/discharge cycle demonstrate a range of characteristic features in responses to the increase in dew point. Up to their respective critical dew point, the voltage curves are nearly identical. This is reflected by the fact that the cell voltage curves for −40 °C dew point are mostly covering the cell voltage curves of the dry reference. In contrast, the cell voltage curves at −20 °C dew point show distinct changes in their voltage profile for both separator types. The first effect is an initial decrease of cell voltage during the first 10–20 mAh $g^{-1}$ of charge throughput ($C_{(I)}$ in Fig. 3(c, d)). A magnified overview of the cell voltage curves during the beginning of charge, including cells assembled at a dew point of −30 °C, can be found in Figs. S2 and S3 in the supplementary material. Following the initial drop in cell voltage, a subsequent relative increase occurs throughout the rest of the first charge ($C_{(II)}$ in Fig. 3(c, d)). This increase is receding towards the end of the charge process for cells assembled with polyolefin separator, thereby not affecting the total charge capacity. However, the voltage increase is more pronounced for cells assembled with ceramic separator, resulting in a reduction in specific charge capacity due to the premature reach of the upper cut-off voltage ($C_{(IIb)}$ in Fig. 3(d)). During discharge, the voltage curves of cells assembled at −20 °C dew point show a premature drop in cell voltage for both separator types, thereby leading to an early realization of the lower cut-off voltage and consequently to a reduced discharge capacity ($D_{(I)}$ in Fig. 3(c, d)).

Fig. 4 displays the anode and cathode potential profiles during the first charge/discharge cycle for cells assembled with polyolefin separator. The evaluation of the individual electrode potentials allows identifying the origin of the observed changes in the cell voltage. The anode potential profile (lower half of Fig. 4) for cells assembled at a dew point of −20 °C shows an increased charge throughput at the beginning of the charge and a premature potential rise at the end of the discharge. Both effects result in a corresponding reduction of cell voltage.

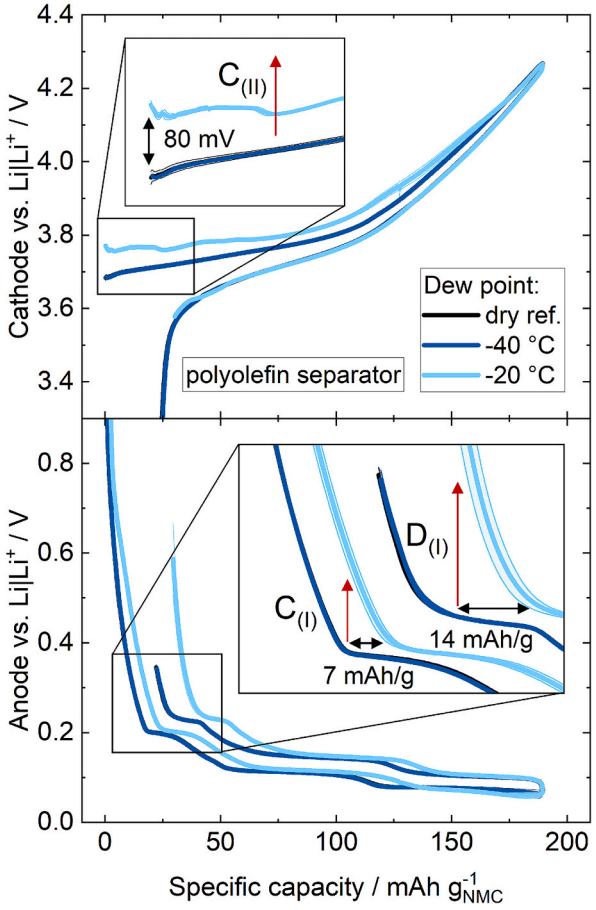


**Fig. 4.** Display of the cathode (top) and anode (bottom) potential profiles, measured against Li|Li + during the first charge/discharge cycle, for exemplary cells assembled with the polyolefin separator. Each potential profile represents the average and standard deviation from four cells.

Accordingly, the features $C_{(I)}$ and $D_{(I)}$ can be assigned to the anode. Consequently, the increase in irreversible capacity measured for cells assembled with polyolefin separators can be attributed entirely to water-induced side reactions at the anode. The features $C_{(I)}$ and $D_{(I)}$ are also present in the cell voltage curves of cells assembled with ceramic separators. This suggests that these side reactions are present for both separator types.

A commonly proposed side-reaction in studies investigating the effect of water contamination on anode performance and SEI-formation is the reduction of water to $H_2$ and $OH^-$. Joho et al. detected the onset of $H_2$ evolution at around 1.3 V vs. Li|$Li^+$ for graphite anodes in 1 M $LiClO_4$ in EC/DMC [58], Bernhard et al. found the onset to be at 1.6 V vs. Li|$Li^+$ for graphite anodes in 1 M LiTFSI in EC/EMC [38] and Kitz et al. determined the onset to be around 2.6 V vs. Li|$Li^+$ for carbon model anodes in 1 M $LiPF_6$ in EC/DEC [30]. The electrolyte composition varies significantly between these studies, which might explain the large scatter of the results. In this study, the first onset of side-reactions for cells with polyolefin separator assembled at a dew point of −20 °C occurs at approximately 1.15 V vs. Li|$Li^+$ followed by a second reaction at around 0.8 V vs. Li|$Li^+$ (see Fig. S4 in Supplementary material). Given that the aforementioned studies employed cyclic voltammetry at low scan rates, while in this work cells are cycled under constant current, a shift towards lower potentials appears reasonable. Furthermore, the presence of VC might further reduce the onset of water reduction compared to electrolyte solutions without additives. It has been demonstrated that a pre-formation of graphite anodes in LP572 electrolyte can effectively reduce the onset and amount of water reduction

[38]. The early reduction of VC during formation may have a similar effect, thereby offering another explanation for the comparatively late onset of side reactions found in this study. Notably, the capacity offset at the end of the last graphite delithiation plateau is approximately twice as high as the offset observed for the first lithiation plateau. Accordingly, only half of the water-induced increase in irreversible capacity can be attributed to the early stages of SEI formation. This suggests that there are ongoing side reactions occurring during the entire first charge/discharge cycle.

A closer examination of the cathode potential profile (upper half of Fig. 4) shows the formation of a distinct peak at the beginning of charge. This leads to an increase in the initial cathode potential from approximately 3.68 V vs Li|Li$^+$ for cells assembled at dry conditions or at a dew point of −40 °C to approximately 3.76 V vs Li|Li$^+$ for cells assembled at a dew point of −20 °C. This effect gradually recedes during the charge process. The rise in cell voltage during the first charge ($C_{(II)}$) can therefore be attributed to the cathode. The changes to the cathode potential profile observed in this study are highly similar to those reported for nickel-rich CAM after exposure to humidity and $CO_2$ [8,9,11,12,14]. The overpotential at the beginning of charge is commonly attributed to the presence of degradation layers, consisting of LiOH and $Li_2CO_3$, on the surface of the CAM after exposure. Jung et al. proposed that the receding overpotential may indicate a decomposition of these degradation layers during the first charge [12]. Consequently, the possibility of CAM ageing must be considered. On the one hand, an exposure to humidified argon (with no or only minimal $CO_2$ content) at a dew point of −20 °C and a temperature of 25 °C would not typically be considered harsh conditions for NMC622. On the other hand, there is little information available on the exact onset of the described phenomena, as most studies on nickel-rich CAM degradation focus on harsh exposure conditions or long exposure times [8,9,11,12]. In this study, the NMC was processed under ambient atmosphere and the resulting cathodes were handled under ambient atmosphere as well. Accordingly, it is plausible to assume, that the NMC exhibited some degree of degradation even before the controlled humidity exposure. This reasoning is supported by the observed high water uptake of the NMC cathodes (see Fig. 2, Section 3.1), which we believe indicates the presence of considerable amounts of hydrate-forming degradation products on the NMC surface. Consequently, it can be hypothesised that the controlled exposure at a dew point of −20 °C might have been sufficient to initiate the additional CAM ageing required to induce measurable changes in the first cycle performance.

However, the considerably more pronounced cell voltage increase observed for cells assembled with ceramic separators (see $C_{(II)}$ in Fig. 3 (c, d)) cannot be explained by CAM ageing alone. The cathodes utilized for both cell types are from the same batch and were prepared, exposed and assembled in parallel. Accordingly, the possibility of additional moisture-induced side reactions triggered by the ceramic separator must be considered. Klein et al. proposed that ceramic particle-coated separators can improve cell performance by scavenging HF and inducing the in situ formation of the additive DFP [59]. However, Rodrigues et al. argued that generic oxide particles can create a hydrolytic cycle that converts HF back to water, thereby facilitating the hydrolysis of $LiPF_6$ [60]. The results presented here indicate that, at high moisture levels, the negative effects of ceramic coatings prevail.

All cells displayed in Fig. 3 were subsequently subjected to a DCIR test and a charge rate test. The results are shown in Fig. 5. The data indicates a comparable pattern to that observed in the first cycle performance. The internal resistance and rate performance are mostly independent from the dew point for low dew points but deteriorate after a certain dew point is surpassed. The respective critical dew point appears to be identical with the critical dew point found for the first cycle performance. The data suggests that the water-induced increase in irreversible capacity observed in the first cycle is accompanied by an increase in internal resistance, which subsequently results in a reduction in rate performance. An increased DCIR as a result of an increased residual moisture content was also reported by Han et al. for automobile 50 Ah pouch cells (Gr/NMC622 with polyolefin separator) [61]. However, the electrode resolved analysis of the DCIR test results (only available for cells with polyolefin separator) does not provide clear indication about the origin of the resistance increase (see Fig. S5 in the supplementary material). The cells assembled with polyolefin separators exhibit a higher cell resistance at low dew points and higher standard deviations in their charge rate performance compared to cells assembled with ceramic separators. A possible explanation for this observation could be the large variation in thickness between the separator types (polyolefin: 220 µm, ceramic: 30 µm), resulting in increased separator resistance for the polyolefin separator.

To validate the DCIR results, additional electrochemical impedance spectroscopy (EIS) tests were performed. These EIS tests were conducted after the DCIR tests for cells assembled at dry conditions and at a dew point of −20 °C. The EIS spectra (see Fig. S6 in the supplementary material) demonstrate a larger high-frequency offset for cells assembled with polyolefin separators compared to cells assembled with ceramic

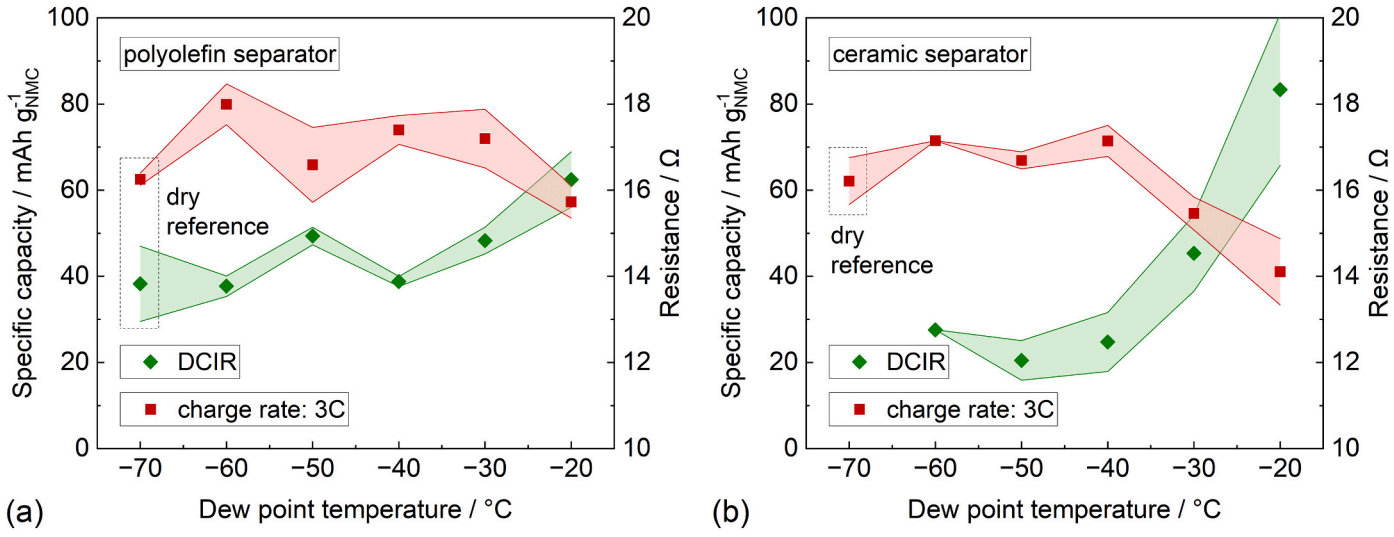


**Fig. 5.** Results of DCIR and charge rate tests for cells assembled with polyolefin separators (a) and ceramic separators (b). The DCIR and charge rate tests were conducted after the initial three formation cycles, using the same cells analysed in Fig. 3. Each data point represents the average and standard deviation of at least three cells (only one cell for ceramic separator at −60 °C (see Section 2.4)).

separators, which is commonly associated with separator resistance [62,63]. Furthermore, cells assembled with ceramic separators under humid conditions show a significant increase of the high-frequency semi-circle (see Table S2 for EIS fitting data). This high frequency semi-circle was associated with the anode SEI by Sabet et al. and Hu et al. [64–66]. An increase of the SEI resistance would be consistent with our observation of water-induced side reactions at the anode. However, the exact attribution of specific processes within EIS spectra is challenging because various interfacial processes with similar time constants are merged within the high- to mid-frequency semi-circles of full-cell EIS spectra [67]. Furthermore, Solchenbach et al. proposed that even when utilizing a reference electrode, it is impossible to distinguish between the SEI and charge transfer resistance of a graphite anode without employing blocking conditions [68]. Consequently, we do not want to imply the assignment of a specific process based only on the available 2-electrode full-cell data.

In order to gain further insight into the long-term effects of increased moisture content in a cell, a second test series was conducted. For these tests, a dew point of −20 °C and −40 °C was chosen as exemplary for dew points that are below and above the critical dew point for cells assembled with a polyolefin separator. Additionally, cells assembled at dry conditions were tested as reference condition. The first cycle performance of the cells of the second test series reproduce the trends found during the dew point screening, namely demonstrating a stable charge/discharge capacity for both the dry reference and a dew point of −40 °C, as well as a reduced discharge capacity (though a stable charge capacity) for a dew point of −20 °C (see Fig. S7 in supplementary material). The corresponding residual moisture of all cell components as measured by KFT is very close to the values gathered during the dew point screening, except for the cathode, which shows a consistent offset towards lower values (see Fig. S1 in the supplementary material).

The results of the cycle life investigation are displayed in Fig. 6. All cells exhibit a high capacity retention of >90 % after 500 cycles (based on the 0.2 C check-up cycles). Cells assembled at a dew point of −40 °C show the best average state of health (SOH: 99 %), followed by the dry reference (SOH: 96 %). The lowest average capacity retention is measured for cells assembled at a dew point of −20 °C (SOH: 93 %). However, the absolute specific capacity after 500 cycles is determined primarily by the capacity differences resulting from the decrease in reversible capacity during the first cycle. Fig. 6 also displays the charge-averaged mean discharge potentials for anode and cathode measured against the lithium reference. The mean anode discharge potential exhibits a consistent offset towards higher potentials for cells assembled at a dew point of −20 °C. This can be attributed to a higher degree of delithiation of the graphite anode, which is a consequence of the higher irreversible losses during formation (see Fig. S8 in Supplementary material). The mean cathode discharge potential remains largely unaffected by the dew point. Jung et al. and Sicklinger et al. found a decreasing mean discharge potential with ongoing cycling for aged NMC811 electrodes, but a stable behaviour for fresh NMC811 electrodes [11,12]. In contrast, the NMC622 electrodes from this work show an almost constant mean discharge potential, independent of the dew point under which the cells are assembled. Nevertheless, all cathodes utilized for the cycle life investigation demonstrate a distinct potential peak at the beginning of the first charge (see Fig. S9 in the Supplementary material), thereby indicating some degree of CAM ageing. As the test series for the cycle life investigation was conducted three months after the dew point screening, it is reasonable to conclude that this phenomenon can potentially be attributed to the effects of CAM ageing during storage. Once more, cells assembled at a dew point of −20 °C demonstrate a consistently higher potential, however the effect is less pronounced in comparison to the first test series. This lends support to the assumption that the NMC used in this study forms additional degradation products during exposure to a dew point of −20 °C. However, the high capacity retention and the stable mean cathode discharge potential indicate that the extent of CAM ageing did not significantly impact the overall cell performance.

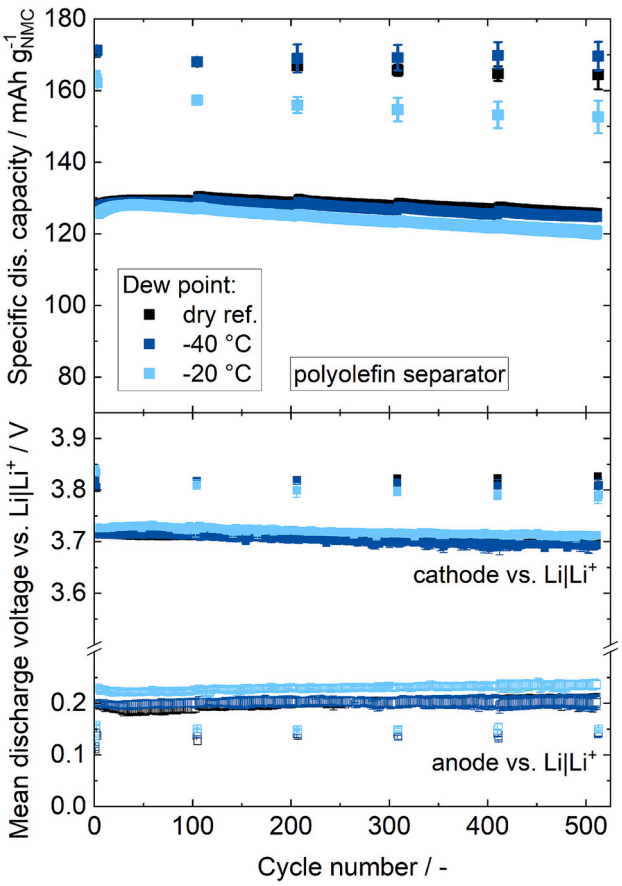


**Fig. 6.** Cycle life investigation of PAT-cells assembled at varying dew points under humidified argon (top) and the respective mean discharge potentials of each electrode measured against Li|Li$^+$ (bottom). All cells were assembled with polyolefin separator. The cycling procedure consists of a formation at 0.1 C, followed by two check-up cycles at 0.2 C. Long term cycling was performed at 1 C for a total of 500 cycles with two check-up cycles at 0.2 C after every 100th cycle. Each data point represents the average and standard deviation of at least three cells.

Overall, the electrochemical characterization of test cells assembled at varying dew points revealed that a critical dew point threshold exists below which no adverse effects on cell performance can be detected. However, the identified critical dew point varied depending on the type of separator used. Above this critical dew point, the primary effect was found to be a decrease in first-cycle reversible capacity that was accompanied by an increase in internal cell resistance and a small decrease in capacity retention after prolonged cycling. The effects on the electrochemical performance found in this study are in good agreement with the results observed by Zheng et al. after injecting water into Gr/NMC-based 18650 cylindrical cells [43]. This suggests that the presented electrochemical indicators of excessive cell moisture are transferable across cell formats.

### *3.3. Correlation between resorbed moisture and electrochemical performance*

It is possible to compare the different separator types and measurement series by correlating the water content of a cell with its electrochemical performance. Fig. 7 presents the first cycle discharge capacity plotted against the total water content of the cell, as determined by KFT and MSB, for each cell tested in this study. The various measurement series display a high degree of consistency. While the test cells exhibit differing critical dew points depending on the type of separator utilized,

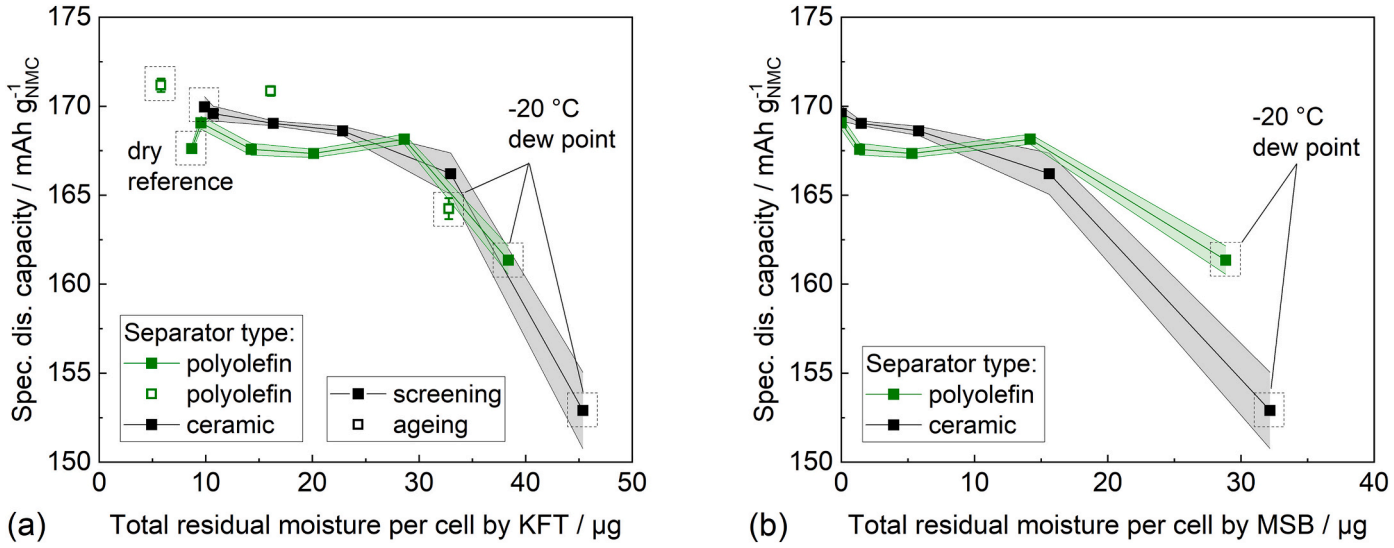


**Fig. 7.** Display of the first cycle discharge capacity plotted against the total residual moisture of each cell tested in this study. The total residual moisture content of a cell was calculated by adding up the residual moisture contents of the anode, cathode and separator, respectively (see Eq. 1, Supplementary material). The values differ significantly depending on whether the KFT data (a) or the MSB data (b) were used as the basis for the calculation. The data for the dry reference cells is absent from the right graph, as the MSB measurements do not yield any results for dew points lower than −60 °C. For all dew points above that, a fit function was employed to generate the water content for each tested dew point.

they display a comparable critical water content. The agreement between the different measurement series appears to be better when the data is plotted over the total water content determined by KFT. Nonetheless, both representations indicate a common critical water content for both separator types. For the first time, this enables to identify a critical water content based on residual moisture analysis of cell components exposed to realistic humidity-exposure histories.

The total residual moisture was deliberately chosen over a relative value to emphasize the difficulty in extrapolating the available data to larger cell formats. In previous studies investigating the impact of water on electrochemical performance, the water content is typically expressed as a ppm value based on the electrolyte mass. However, this unit is not suitable for comparing laboratory-scale cell formats, such as the PAT-Cells used in this study, with larger-scale cells, given that they display largely different electrolyte to AM ratios [69,70]. The results of the electrochemical characterization presented in this study indicate that an increase in residual moisture is associated with an increase in irreversible capacity. It is reasonable to assume that the increase in irreversible capacity is accompanied by a loss of active lithium. This suggests that relating the total residual moisture to the cathode AM mass could be a promising unit of comparison. However, as all experiments in this work were conducted with the same electrode material, it is not possible to verify this assumption based on the available data set. The first cycle discharge capacities displayed in Fig. 7 were also plotted against the electrolyte-specific moisture and the CAM-specific moisture, allowing the interested reader to make a more accurate comparison with the existing literature (see Fig. S10, Supplementary material). However, it must be stressed that a direct comparison between results obtained for different cell formats (e.g. PAT-Cell and multilayer pouch cell) and by employing different methods to introduce water into the cell (e.g. direct injection into the electrolyte vs. increased residual moisture in cell components) is unlikely to yield meaningful outcomes.

On a more fundamental level, it is also worth exploring the plausibility of the critical residual moisture values determined in this study. Indeed, the good agreement between cells assembled with the polyolefin and the ceramic separator may also be a mere anomaly and therefore misleading. In fact, it would be an unusual coincidence if the KFT parameters selected for this study truly reflected the electrochemically active amount of water in each cell component. With electrochemically active we understand all water that is available for reactions with other cell components under battery operation conditions. Depending on the measurement method and the exact measurement conditions, different water contents can be determined for the same material [27,37]. The critical residual moisture content for the cells tested in this work is approximately 30 µg (or around 800 ppm of CAM-specific moisture, see supplementary materials), if the KFT results are used as the reference value. However, if the water content determined by MSB is employed, the critical water content is only at around half that value. Therefore, it is always necessary to state the exact measurement method together with the critical residual moisture content.

To the best of our knowledge, there is no existing literature that addresses the question of how much water is electrochemically active within common battery materials at different residual moisture loadings. The residual moisture within battery materials can be classified into three categories of sorption mechanisms (see Fig. 8). These are: (i) water adsorbed to the surface, (ii) water absorbed into the material and (iii) formation of hydrates. For the purpose of this discussion, the term “residual moisture” refers solely to water that is still present in its molecular form. It can be assumed that adsorbed and absorbed water will transfer into the electrolyte once the material surface is wetted until the chemical potentials between water on the surface or in the polymer and water in the electrolyte are in equilibrium. However, there is limited information available regarding the chemical potentials of water in each of the components. The single largest source of water inside a battery is the water that is stored inside the CMC binder, yet we are not aware of any literature reporting how much of that water transfers into the electrolyte under realistic water loadings and real-world battery operating conditions. For very low water loadings it was even shown that the presence of CMC can stabilize $LiPF_6$-based electrolytes against water sources by scavenging HF from the electrolyte [71]. The situation is even less clear regarding water that is more strongly bound, such as hydrates. Hydrates have only recently been considered as a potential source of water in LIB [36]. In general, hydrates require some level of thermal activation to desorb from their host material (e.g. LiOH). However, if the host material itself decomposes, as has been proposed for the LiOH-containing surface layers on top of Ni-rich CAM during the first charge [12], the water may be released at a much lower temperature. Notably, the cathodes used for cycle life investigation in this study showed a

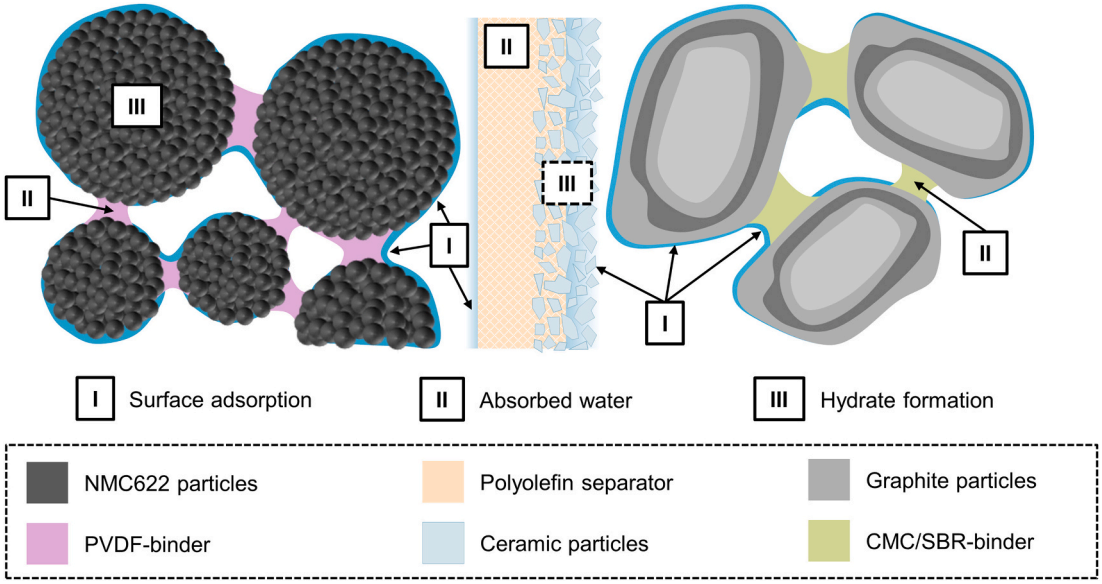


**Fig. 8.** Overview of sorption mechanisms that contribute to the residual moisture within the anode, cathode and separator. Surface adsorption is a phenomenon that occurs in all materials, whereas water absorption is predominantly observed in polymeric materials, such as binder or separator membrane/non-woven. The formation of hydrates was proposed for NMC, and it may be reasonably assumed that it also occurs in ceramic particles used as separator coatings. In this schematic, only sorption mechanisms in which water remains in its molecular form are considered.

consistently lower water content compared to the cathodes used for dew point screening. The offset in water content can only be explained by different levels of hydrate formation during sample handling. The consistently higher first cycle discharge capacities of these cells provide a first indication that hydrates may influence cell performance.

## 4. Conclusion

This study investigated the moisture resorption behaviour and resulting electrochemical performance of graphite anodes, NMC cathodes and two types of separator (one polyolefin and one with a ceramic coating) under industrially relevant levels of humidity. Two different analytic techniques, namely Karl Fischer titration (KFT) and magnetic suspension balance (MSB), were utilized to examine the moisture uptake behaviour. Despite a comparable humidity-exposure history of the samples, a consistent offset was observed between the results obtained from KFT and MSB. Our findings indicate that this offset is predominantly a function of the different measurement temperatures (120 °C for KFT vs. 25 °C for MSB). It is our view that the formation of hydrates and the process of chemical sorption should be taken into account when considering the moisture resorption behaviour of NMC and ceramic particle-containing separators.

The impact of humidity on electrochemical performance was examined by assembling test cells utilizing solely moisture-saturated cell components. The assembly of the cells and the preparation of KFT samples were conducted in parallel to ensure a high degree of comparability between the two methods. The test results indicate a stable performance for low dew points and a decline in performance after a critical dew point is exceeded. The critical dew point was found to be at −40 °C for cells assembled with a ceramic separator and −30 °C for cells employing a polyolefin separator. The primary influence on electrochemical performance was determined to be an increase in irreversible capacity during formation, which could be attributed to water-induced side reactions at the anode. For cells assembled with ceramic separators this was accompanied by a decrease in initial charge capacity, which indicates the possibility of additional side reactions triggered by the separator. Furthermore, an increase in internal resistance and a corresponding reduction in charge rate capability were observed in cells assembled above the critical dew point. The cycle life investigation revealed only a minor impact of the dew point on ageing behaviour. Even above the critical dew point, the state of health after 500 cycles was primarily influenced by the increase in irreversible capacity during the first cycle.

By combining the residual moisture data with the results from the electrochemical characterization, it was possible to identify a common critical water content for all cells tested in this work. This makes it possible, for the first time, to define a critical residual moisture threshold. However, the value differs depending on the method used to determine the water content. There is a gap in knowledge regarding how much of the water measured by different methods (using varying parameters) is electrochemically active within the battery cell. It seems reasonable to assume that not all the water that can be measured is also available for (electro-)chemical reactions under battery operation conditions. The findings of this study underline the need for further research to differentiate the impact of differently bound water on cell performance. At a fundamental level, a deeper understanding of the transfer of water between cell components and electrolyte would be highly valuable. On a practical level, it is important to investigate the effects of different electrode parameters and compositions, as well as the transferability to different cell formats.

## CRediT authorship contribution statement

**Hans Fenske:** Writing – review & editing, Writing – original draft, Investigation, Formal analysis, Conceptualization. **Thilo Heckmann:** Writing – review & editing, Writing – original draft, Investigation, Formal analysis, Conceptualization. **Peter Michalowski:** Writing – review & editing, Supervision. **Philip Scharfer:** Writing – review & editing, Supervision, Funding acquisition, Conceptualization. **Wilhelm Schabel:** Writing – review & editing, Supervision. **Arno Kwade:** Writing – review & editing, Supervision.

## Declaration of generative AI and AI-assisted technologies in the writing process

During the preparation of this work, the authors used DeepL (DeepL SE) to improve readability and clarity. The authors reviewed and edited the content after usage and take full responsibility for the content of the

publication.

## Declaration of competing interest

The authors declare that they have no known competing financial interests or personal relationships that could have appeared to influence the work reported in this paper.

## Acknowledgments

The authors gratefully acknowledge the financial support by the German Federal Ministry of Education and Research (BMBF) within the research project Epic (03XP0295B). Furthermore, the authors would like to thank Max-Wolfram von Horstig for the automation of cycling data evaluation, Hai Linh Briese for experimental support and Jessica Gerstenberg for her assistance in analysing the EIS spectra.

## Appendix A. Supplementary data

Supplementary data to this article can be found online at https://doi.org/10.1016/j.est.2025.116238.

## Data availability

Data will be made available on request.

## References

[1] A. Kwade, W. Haselrieder, R. Leithoff, A. Modlinger, F. Dietrich, K. Droeder, Nat. Energy 3 (2018) 290–300, https://doi.org/10.1038/s41560-018-0130-3.
[2] M. Vogt, K. Koch, A. Turetskyy, F. Cerdas, S. Thiede, C. Herrmann, Proc. CIRP 98 (2021) 157–162, https://doi.org/10.1016/j.procir.2021.01.023.
[3] S. Ahmed, P.A. Nelson, D.W. Dees, J. Power Sources 326 (2016) 490–497, https://doi.org/10.1016/j.jpowsour.2016.06.107.
[4] U. Heider, R. Oesten, M. Jungnitz, J. Power Sources 81–82 (1999) 119–122, https://doi.org/10.1016/S0378-7753(99)00142-1.
[5] D. Strmcnik, I.E. Castelli, J.G. Connell, D. Haering, M. Zorko, P. Martins, P. P. Lopes, B. Genorio, T. Østergaard, H.A. Gasteiger, F. Maglia, B.K. Antonopoulos, V.R. Stamenkovic, J. Rossmeisl, N.M. Markovic, Nat. Catal. 1 (2018) 255–262, https://doi.org/10.1038/s41929-018-0047-z.
[6] X. Cui, F. Tang, Y. Zhang, C. Li, D. Zhao, F. Zhou, S. Li, H. Feng, Electrochim. Acta 273 (2018) 191–199, https://doi.org/10.1016/j.electacta.2018.03.138.
[7] W. Liu, H. Cai, D. Liu, R. Hua, H. Gao, R. Zhang, H. Tang, J. Li, D. Qu, Int. J. Energy Res. 46 (2022) 7988–7995, https://doi.org/10.1002/er.7700.
[8] I.A. Shkrob, J.A. Gilbert, P.J. Phillips, R. Klie, R.T. Haasch, J. Bareño, D. P. Abraham, J. Electrochem. Soc. 164 (2017) A1489–A1498, https://doi.org/10.1149/2.0861707jes.
[9] Z. Chen, J. Wang, J. Huang, T. Fu, G. Sun, S. Lai, R. Zhou, K. Li, J. Zhao, J. Power Sources 363 (2017) 168–176, https://doi.org/10.1016/j.jpowsour.2017.07.087.
[10] J.-H. Park, J.-K. Park, J.-W. Lee, Bull. Kor. Chem. Soc. 37 (2016) 344–348, https://doi.org/10.1002/bkcs.10679.
[11] J. Sicklinger, M. Metzger, H. Beyer, D. Pritzl, H.A. Gasteiger, J. Electrochem. Soc. 166 (2019) A2322–A2335, https://doi.org/10.1149/2.0011912jes.
[12] R. Jung, R. Morasch, P. Karayaylali, K. Phillips, F. Maglia, C. Stinner, Y. Shao-Horn, H.A. Gasteiger, J. Electrochem. Soc. 165 (2018) A132–A141, https://doi.org/10.1149/2.0401802jes.
[13] L. Zhang, E.A. Müller Gubler, C.-W. Tai, Ł. Kondracki, H. Sommer, P. Novák, M. El Kazzi, S. Trabesinger, ACS Appl. Mater. Interfaces 14 (2022) 13240–13249, https://doi.org/10.1021/acsami.1c23128.
[14] N.V. Faenza, L. Bruce, Z.W. Lebens-Higgins, I. Plitz, N. Pereira, L.F.J. Piper, G. G. Amatucci, J. Electrochem. Soc. 164 (2017) A3727–A3741, https://doi.org/10.1149/2.0921714jes.
[15] Y. Lin, M. Xu, Y. Tian, W. Fan, L. Yu, W. Li, Mater. Chem. Phys. 211 (2018) 200–205, https://doi.org/10.1016/j.matchemphys.2018.02.031.
[16] L. Zou, Y. He, Z. Liu, H. Jia, J. Zhu, J. Zheng, G. Wang, X. Li, J. Xiao, J. Liu, J.-G. Zhang, G. Chen, C. Wang, Nat. Commun. 11 (2020) 3204, https://doi.org/10.1038/s41467-020-17050-6.
[17] M. Lechner, S. Wölfl, E. Kurz, R. Daub, J. Power Sources 626 (2025) 235661, https://doi.org/10.1016/j.jpowsour.2024.235661.
[18] J.C. Eser, B. Deichmann, T. Wirsching, P.G. Weidler, P. Scharfer, W. Schabel, Langmuir 36 (2020) 6193–6201, https://doi.org/10.1021/acs.langmuir.0c00704.
[19] J.C. Eser, T. Wirsching, P.G. Weidler, A. Altvater, T. Börnhorst, J. Kumberg, G. Schöne, M. Müller, P. Scharfer, W. Schabel, Energy Technol. 8 (2020), https://doi.org/10.1002/ente.201801162.
[20] M. Kosfeld, B. Westphal, A. Kwade, J. Energy Storage 57 (2023) 106174, https://doi.org/10.1016/j.est.2022.106174.
[21] F. Huttner, A. Marth, J.C. Eser, T. Heckmann, J. Mohacsi, J.K. Mayer, P. Scharfer, W. Schabel, A. Kwade, Batteries Supercaps 4 (2021) 1499–1515, https://doi.org/10.1002/batt.202100088.
[22] F. Huttner, A. Diener, T. Heckmann, J.C. Eser, T. Abali, J.K. Mayer, P. Scharfer, W. Schabel, A. Kwade, J. Electrochem. Soc. 168 (2021) 90539, https://doi.org/10.1149/1945-7111/ac24bb.
[23] E.R. Logan, H. Hebecker, A. Eldesoky, A. Luscombe, M.B. Johnson, J.R. Dahn, J. Electrochem. Soc. 167 (2020) 130543, https://doi.org/10.1149/1945-7111/abbbbe.
[24] D. Yang, X. Li, N. Wu, W. Tian, Electrochim. Acta 188 (2016) 611–618, https://doi.org/10.1016/j.electacta.2015.12.063.
[25] J. Li, C. Daniel, S.J. An, D. Wood, MRS Adv. 1 (2016) 1029–1035, https://doi.org/10.1557/adv.2016.6.
[26] S. Radloff, R.-G. Scurtu, G. Carbonari, M. Hölzle, T. Diemant, M. Bozorgchenani, F. Klein, M. Wohlfahrt-Mehrens, J. Power Sources 580 (2023) 233314, https://doi.org/10.1016/j.jpowsour.2023.233314.
[27] M. Kosfeld, B. Westphal, A. Kwade, J. Energy Storage 51 (2022) 104398, https://doi.org/10.1016/j.est.2022.104398.
[28] D. Aurbach, B. Markovsky, A. Shechter, Y. Ein-Eli, H. Cohen, J. Electrochem. Soc. 143 (1996) 3809–3820, https://doi.org/10.1149/1.1837300.
[29] D. Aurbach, B. Markovsky, G. Salitra, E. Markevich, Y. Talyossef, M. Koltypin, L. Nazar, B. Ellis, D. Kovacheva, J. Power Sources 165 (2007) 491–499, https://doi.org/10.1016/j.jpowsour.2006.10.025.
[30] P.G. Kitz, P. Novák, E.J. Berg, ACS Appl. Mater. Interfaces 12 (2020) 15934–15942, https://doi.org/10.1021/acsami.0c01642.
[31] T. Hettesheimer, C. Neef, I. Rosellón Inclán, S. Link, T. Schmaltz, F. Schuckert, A. Stephan, M. Stephan, A. Thielmann, L. Weymann, T. Wicke, Lithium-Ion Battery Roadmap — Industrialization Perspectives toward 2030, Fraunhofer-Gesellschaft, 2022.
[32] S. Link, C. Neef, T. Wicke, Batteries 9 (2023) 261, https://doi.org/10.3390/batteries9050261.
[33] H. Chen, T. Ericson, R.H. Temperton, I. Källquist, H. Liu, C.N. Eads, A. Mikheenkova, M. Andersson, E. Kokkonen, W.R. Brant, M. Hahlin, ACS Appl. Energy Mater. 6 (2023) 11458–11467, https://doi.org/10.1021/acsaem.3c01621.
[34] Q. Dong, R. Yi, J. Qi, Y. Shen, L. Chen, Chin. Phys. Lett. 39 (2022) 38201, https://doi.org/10.1088/0256-307X/39/3/038201.
[35] T. Heckmann, J.C. Eser, A. Altvater, N. Streller, P. Scharfer, W. Schabel, Energy Technol. 11 (2023), https://doi.org/10.1002/ente.202200859.
[36] T. Heckmann, L. Madlindl, P. Scharfer, W. Schabel, A.C.S. Appl, ACS Appl. Energy Mater. 7 (2024) 1882–1889, https://doi.org/10.1021/acsaem.3c02976.
[37] M. Stich, N. Pandey, A. Bund, J. Power Sources 364 (2017) 84–91, https://doi.org/10.1016/j.jpowsour.2017.08.009.
[38] R. Bernhard, M. Metzger, H.A. Gasteiger, J. Electrochem. Soc. 162 (2015) A1984–A1989, https://doi.org/10.1149/2.0191510jes.
[39] M. Metzger, B. Strehle, S. Solchenbach, H.A. Gasteiger, J. Electrochem. Soc. 163 (2016) A1219–A1225, https://doi.org/10.1149/2.0411607jes.
[40] J.C. Burns, N.N. Sinha, G. Jain, H. Ye, C.M. VanElzen, E. Scott, A. Xiao, W. M. Lamanna, J.R. Dahn, J. Electrochem. Soc. 160 (2013) A2281–A2287, https://doi.org/10.1149/2.101311jes.
[41] J.C. Burns, N.N. Sinha, G. Jain, H. Ye, C.M. VanElzen, E. Scott, A. Xiao, W. M. Lamanna, J.R. Dahn, J. Electrochem. Soc. 161 (2014) A247–A255, https://doi.org/10.1149/2.024403jes.
[42] D.J. Xiong, R. Petibon, L. Madec, D.S. Hall, J.R. Dahn, J. Electrochem. Soc. 163 (2016) A1678–A1685, https://doi.org/10.1149/2.0901608jes.
[43] L.-Q. Zheng, S.-J. Li, H.-J. Lin, Y.-Y. Miao, L. Zhu, Z.-J. Zhang, Russ. J. Electrochem. 50 (2014) 904–907, https://doi.org/10.1134/S1023193514090122.
[44] U. Langklotz, M. Schneider, A. Michaelis, J. Ceram. Sci. Technol. (2012) 69–76, https://doi.org/10.4416/JCST2012-00036.
[45] P. Handel, G. Fauler, K. Kapper, M. Schmuck, C. Stangl, R. Fischer, F. Uhlig, S. Koller, J. Power Sources 267 (2014) 255–259, https://doi.org/10.1016/j.jpowsour.2014.05.080.
[46] A.R. Schuer, M. Kuenzel, S. Yang, M. Kosfeld, F. Mueller, S. Passerini, D. Bresser, J. Power Sources 525 (2022) 231111, https://doi.org/10.1016/j.jpowsour.2022.231111.
[47] F. Baakes, D. Witt, U. Krewer, Chem. Sci. 14 (2023) 13783–13798, https://doi.org/10.1039/d3sc04186g.
[48] X. Yang, R. Kleinrahm, M.O. McLinden, M. Richter, Int. J. Thermophys. 44 (2023) 1666, https://doi.org/10.1007/s10765-023-03269-0.
[49] Y. Tang, X. Wang, Y. Wen, X. Zhou, Z. Li, Ind. Eng. Chem. Res. 59 (2020) 6219–6225, https://doi.org/10.1021/acs.iecr.0c00441.
[50] A. Raje, P. Georgopanos, J. Koll, J. Lillepärg, U.A. Handge, V. Abetz, Polymers 15 (2022), https://doi.org/10.3390/polym15010118.
[51] Z. Lu, J. Zhang, H. He, L. Du, C. Hang, Inorg. Chem. Front. 4 (2017) 736–740, https://doi.org/10.1039/C6QI00616G.
[52] International Energy Agency, Global EV outlook 2023: trends in batteries. https://www.iea.org/reports/global-ev-outlook-2023/trends-in-batteries accessed 9 January 2025.
[53] J. Kasnatscheew, T. Placke, B. Streipert, S. Rothermel, R. Wagner, P. Meister, I. C. Laskovic, M. Winter, J. Electrochem. Soc. 164 (2017) A2479–A2486, https://doi.org/10.1149/2.0961712jes.
[54] W. Schabel, I. Mamaliga, M. Kind, Chem. Ing. Tech. 75 (2003) 36–41, https://doi.org/10.1002/cite.200390017.
[55] F. Thurner, M. Stietz, Chem. Eng. Process. Process Intensif. 18 (1984) 333–340, https://doi.org/10.1016/0255-2701(84)87010-5.
[56] Y. Liu, Y. Zhu, Y. Cui, Nat. Energy 4 (2019) 540–550, https://doi.org/10.1038/s41560-019-0405-3.

[57] M. Weiss, R. Ruess, J. Kasnatscheew, Y. Levartovsky, N.R. Levy, P. Minnmann, L. Stolz, T. Waldmann, M. Wohlfahrt-Mehrens, D. Aurbach, M. Winter, Y. Ein-Eli, J. Janek, Adv. Energy Mater. 11 (2021) A1060, https://doi.org/10.1002/aenm.202101126.
[58] F. Joho, B. Rykart, R. Imhof, P. Novák, M.E. Spahr, A. Monnier, J. Power Sources 81–82 (1999) 243–247, https://doi.org/10.1016/S0378-7753(99)00195-0.
[59] S. Klein, J.M. Wrogemann, S. van Wickeren, P. Harte, P. Bärmann, B. Heidrich, J. Hesper, K. Borzutzki, S. Nowak, M. Börner, M. Winter, J. Kasnatscheew, T. Placke, Adv. Energy Mater. 12 (2022) 214, https://doi.org/10.1002/aenm.202102599.
[60] M.-T.F. Rodrigues, C. Liao, K. Kalaga, I.A. Shkrob, D.P. Abraham, A.C.S. Appl, ACS Appl. Energy Mater. 2 (2019) 5380–5385, https://doi.org/10.1021/acsaem.9b00976.
[61] X. Han, S. Xia, J. Cao, C. Wang, M.-G. Chen, Int. J. Electrochem. Sci. 16 (2021) 210554, https://doi.org/10.20964/2021.05.54.
[62] W. Choi, H.-C. Shin, J.M. Kim, J.-Y. Choi, W.-S. Yoon, J. Electrochem. Sci. Technol. 11 (2020) 1–13, https://doi.org/10.33961/jecst.2019.00528.
[63] R. Morasch, J. Keilhofer, H.A. Gasteiger, B. Suthar, J. Electrochem. Soc. 168 (2021) 80519, https://doi.org/10.1149/1945-7111/ac1892.
[64] P. Shafiei Sabet, D.U. Sauer, J. Power Sources 425 (2019) 121–129, https://doi.org/10.1016/j.jpowsour.2019.03.068.
[65] P. Shafiei Sabet, A.J. Warnecke, F. Meier, H. Witzenhausen, E. Martinez-Laserna, D. U. Sauer, J. Power Sources 449 (2020) 227369, https://doi.org/10.1016/j.jpowsour.2019.227369.
[66] W. Hu, Y. Peng, Y. Wei, Y. Yang, J. Phys. Chem. C 127 (2023) 4465–4495, https://doi.org/10.1021/acs.jpcc.3c00033.
[67] N. Meddings, M. Heinrich, F. Overney, J.-S. Lee, V. Ruiz, E. Napolitano, S. Seitz, G. Hinds, R. Raccichini, M. Gaberšček, J. Park, J. Power Sources 480 (2020) 228742, https://doi.org/10.1016/j.jpowsour.2020.228742.
[68] S. Solchenbach, X. Huang, D. Pritzl, J. Landesfeind, H.A. Gasteiger, J. Electrochem. Soc. 168 (2021) 110503, https://doi.org/10.1149/1945-7111/ac3158.
[69] A. Smith, P. Stüble, L. Leuthner, A. Hofmann, F. Jeschull, L. Mereacre, Batteries Supercaps 6 (2023) 5176, https://doi.org/10.1002/batt.202300080.
[70] M.D.L. Garayt, M.B. Johnson, L. Laidlaw, M.A. McArthur, S. Trussler, J.E. Harlow, J.R. Dahn, C. Yang, J. Electrochem. Soc. 170 (2023) 80516, https://doi.org/10.1149/1945-7111/aceffc.
[71] S. Wiemers-Meyer, S. Jeremias, M. Winter, S. Nowak, Electrochim. Acta 222 (2016) 1267–1271, https://doi.org/10.1016/j.electacta.2016.11.100.